Observation of Flat Bands in Gated Semiconductor Artificial Graphene

Lingjie Du,[1,2,*] Ziyu Liu,[3] Shalom J. Wind,[2] Vittorio Pellegrini,[4] Ken W. West,[5] Saeed Fallahi,[6] Loren N. Pfeiffer,[5] Michael J. Manfra,[6] and Aron Pinczuk[2,3,†]

[1]*School of Physics, and National Laboratory of Solid State Microstructures, Nanjing University, Nanjing 210093, China*
[2]*Department of Applied Physics and Applied Mathematics, Columbia University, New York, New York 10027, USA*
[3]*Department of Physics, Columbia University, New York, New York 10027, USA*
[4]*Istituto Italiano di Tecnologia, Graphene Labs, Via Morego 30, I-16163 Genova, Italy*
[5]*Department of Electrical Engineering, Princeton University, Princeton, New Jersey 08544, USA*
[6]*Department of Physics and Astronomy, and School of Materials Engineering, and School of Electrical and Computer Engineering, Purdue University, West Lafayette, Indiana 47907, USA*

(Received 17 October 2020; accepted 15 February 2021; published 12 March 2021)

Flat bands near M points in the Brillouin zone are key features of honeycomb symmetry in artificial graphene (AG) where electrons may condense into novel correlated phases. Here we report the observation of van Hove singularity doublet of AG in GaAs quantum well transistors, which presents the evidence of flat bands in semiconductor AG. Two emerging peaks in photoluminescence spectra tuned by backgate voltages probe the singularity doublet of AG flat bands and demonstrate their accessibility to the Fermi level. As the Fermi level crosses the doublet, the spectra display dramatic stability against electron density, indicating interplays between electron-electron interactions and honeycomb symmetry. Our results provide a new flexible platform to explore intriguing flat band physics.

DOI: 10.1103/PhysRevLett.126.106402

In two-dimensional electron systems (2DES), dispersionless electron bands (flat bands) present divergent density of states (DOS) [known as van Hove singularity (vHS)]. As the Fermi level (E_F) crosses the vHS, electrons are usually unstable against the formation of new quantum phases such as novel superconducting states and spin or charge density waves [1–3]. Nevertheless, after extensive search, only limited electron structures have vHSs accessible for E_F. One famous example is Landau levels in quantum Hall effect. Another is flat bands in "moiré superlattices of twisted atomic layers [4,5], where superconductivity has been observed when E_F overlaps a flat band of twisted-bilayer graphene [6]. In semiconductor artificial graphene (AG), pairs of flat bands with honeycomb symmetry are predicted near the Brillouin zone (BZ) M points [7–9]. Electron states in the semiconductor systems could be controlled by gating methods [10], giving possibilities of bringing E_F to vHSs in semiconductor AG.

Semiconductor AG has electron band structures that could be tuned by honeycomb-lattice periods [9,11,12]. Linearly dispersing Dirac bands have been observed in AG based on GaAs quantum wells (QWs) [12]. Later the nanofabrication of antidots in AG provides a key element to suppress the impact of processing disorder on electrons [9]. However, probes of vHSs in the DOS of semiconductor AG that are essential to confirm the presence of flat bands have not been realized. Scanning tunneling methods offered experimental accesses to vHSs in the DOS of twisted-bilayer graphene [13] and to Dirac fermions in molecular AG [14], but are difficult to apply on semiconductor AG buried under insulating layers. Optical emission (photoluminescence, PL) could offer direct probes of the electron DOS in GaAs AG. PL spectra are from optical recombination transitions between mobile electrons in conduction bands (CB) and weakly photoexcited holes in valence bands (VB). Holes in GaAs AG have nearly dispersionless VB, so that the line shapes of PL spectra offer direct insights on the electron DOS [15–17]. The evolution of PL spectra as a function of E_F, enabled by gating semiconductor AG, would distinguish emerging optical characteristics.

In this Letter we report the evidence of flat bands in carrier-density-dependent PL experiments in semiconductor AG on a GaAs QW where the electron density n_e is tuned by a voltage V_b applied to a backgate fabricated in the device. PL spectra probe a striking emission doublet that occurs when E_F crosses the flat band doublet in AG. The energy splitting of the characteristic PL doublet is well described by the DOS singularities of flat bands near M points. The carrier-density dependence of the PL doublet further identifies it as the vHS doublet of flat bands. The recombination energies and line shapes of emission doublet remain constant over a wide range of V_b, revealing remarkable interplay between Coulomb interactions and honeycomb symmetry of electrons. The tunability of E_F to access flat bands would enable explorations of novel quantum phases in nanofabricated semiconductor devices.

Figure 1(a) describes the backgated AG device structure. A high-quality 2D electron gas is confined in a 25 nm single GaAs/$Al_xGa_{1-x}As$ QW modulation doped with Si

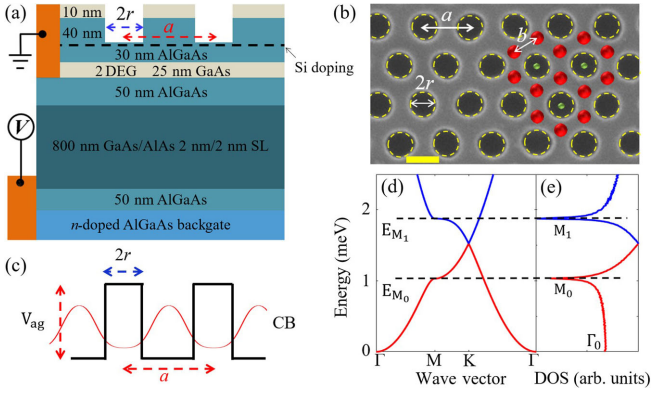

FIG. 1. (a) Cross-section view of the AG device showing the heterostructure layer sequence with triangular-antidot lattices imprinted on a GaAs QW. Dimensions are not to scale. The antidot radius is r and the period is a. SL is for superlattice. (b) Scanning electron microscopy micrographs of AG lattices with $a = 70$ nm and $r = 20$ nm. The dashed circles mark antidots. The variation of r is below 5 nm. The scale bar is 50 nm. Red large dots indicate maximum positions of electron wave functions. Green small dots indicate positions of photoexcited holes. Holes are in a triangular lattice with a large effective mass, resulting in nearly dispersionless VB. (c) Muffin-tin AG potential and wave functions in the single-particle approximation for electrons. Panels (d) and (e) show the two lowest AG bands and DOS with the parameters in (b). In (e), the Γ-point onset, the singularity from a lower flat band, and the singularity from an upper flat band are marked as Γ_0, M_0, and M_1, respectively. E_{M1} and E_{M0} mark energies of the upper and lower flat band.

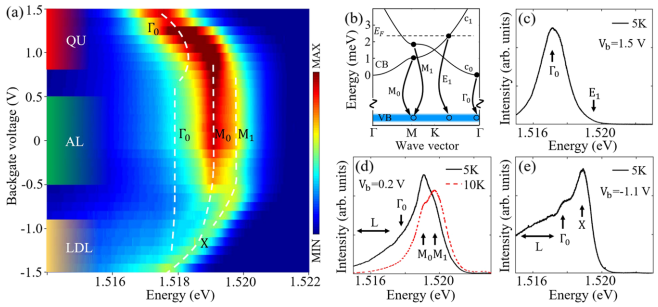

FIG. 2. (a) PL spectra as a function of V_b at 5 K. PL spectra were excited by tunable emissions from a Ti:sapphire laser focused to a spot of ~100 μm onto the AG device. Incident power was 3–10 μW. Dashed lines mark PL peaks as Γ_0, M_0, M_1, and X. The color code is linear with intensity. (b) Optical transitions in PL peaks between electron (dot) and hole (circle) states. E_1 represents the energy of transitions at E_F. The two lowest AG CBs are marked as c_0 and c_1. (c) PL trace for $V_b = 1.5$ V at 5 K. The difference between Γ_0 and E_1 yields a determination of E_F. (d) The black (dotted red) line represents PL trace under $V_b = 0.2$ V at 5 K (10 K). L indicates the transitions from localized states. (e) PL trace under $V_b = -1.1$ V at 5 K.

grown by molecular beam epitaxy [10,18]. The layer sequence and their composition have been optimized for optical measurements. An n^+ $Al_xGa_{1-x}As$ layer serves as a backgate to tune n_e. As shown in Fig. 1(b), a triangular-antidot lattice with period $a = 70$ nm (equivalent honeycomb-dot-lattice period $b = 35$ nm) is patterned on the QW by means of 80 keV e-beam lithography followed by reactive ion etching [9,19]. The AG lattice is on a mesa fabricated by wet etching with phosphoric acid and hydrogen peroxide. Ge/Pd/Au alloy contacts are connected to the AG lattice and the backgate. The AG device is placed in an optical cryostat for measurements with a base temperature of 5 K. Figure 1(d) shows calculated AG band structures with the device parameters, where a prominent feature is a pair of flat bands around M points. Figure 1(e) shows that the flat bands have vHSs in the DOS in six equivalent valleys at M points.

Figure 2(a) shows V_b dependence of PL spectra and Fig. 2(b) describes conduction-to-valence-band transitions active in the spectra. Holes in VB are subject to impact of disorder, because their wave functions have maxima under antidots [green circles in Fig. 1(b)] [9]. Three regions of V_b are highlighted and their typical PL spectra are shown in Figs. 2(c)–2(e). The quasiuniform (QU) region [red in Fig. 2(a)] is for $V_b > 0.8$ V. PL spectra in this region are dominated by a single broad peak Γ_0 at energies redshifting with increasing V_b [see Fig. 2(c)]. The AG quantum limit (AL) region [green in Fig. 2(a)] is for $-0.5 < V_b < 0.5$ V, which is defined by the emergence of a strong PL doublet (M_0 and M_1) that is largely unchanged [see Fig. 2(d)]. The low-density limit (LDL) region [yellow in Fig. 2(a)] is for $V_b < -0.9$ V, where the PL doublet finally merges into one main band (X) [see Fig. 2(e)].

Onset Γ_0 in the three regions is assigned to optical transitions from c_0 band electrons to VB holes near the Γ point of the BZ. The broad PL band in region QU is similar to that from uniform 2DES in unpatterned QWs, whose line shape yields an accurate estimation of E_F [15–17]. The evaluation of E_F as a function of V_b in Fig. 3 estimates population changes of AG states. It shows that at the start of region AL (0.5 V) E_F is near M_1 singularity and moves toward M_0 singularity at $V_b < -0.1$ V. Remarkably, E_F always stays between the singularity doublet in region AL. This implies that in region AL at 5 K optical transitions from the M_0 singularity make the largest contribution to PL spectra.

At $V_b = 0.5$ V, n_e is estimated as 5.3×10^{10} cm^{-2} and E_F (~1.9 meV) is below the AG potential 5 meV [9]. Then electrons are largely confined in the red circles [unetched area in Fig. 1(b)] that have honeycomb symmetry. In region AL the intensity step at 1518 meV is continuously linked to onset Γ_0 in region QU and thus attributed to optical recombination by electrons at the Γ point (see Fig. S1 of Supplemental Material [20]). Two peaks marked as M_0 and M_1 in Fig. 2(d) are the strongest PL features in region AL. The line shapes of PL spectra in region AL show significant difference from ones in region QU and ones in the unpatterned QW (see Fig. S2 of Supplemental Material [20]). Figure 2(d) shows that the

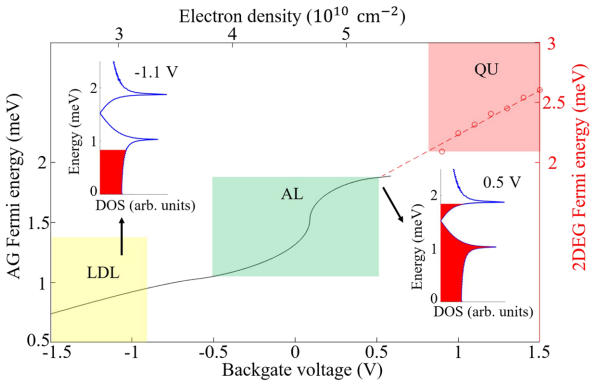

FIG. 3. E_F as a function of V_b (n_e). Red open circles and the red dashed line represent E_F determined from PL spectra and their linear extension. In region QU, E_F is transferred to n_e from difference between Γ_0 and E_1 as shown in Fig. 2(b) since electrons are quasi-two-dimensional. Because V_b tunes n_e linearly, it determines other n_e marked in the top axis. The black line represents the calculated E_F. Three regions in red, green, and yellow are those defined in Fig. 2(a). Insets: schematic representations of AG band populations at $V_b = -1.1$ and 0.5 V.

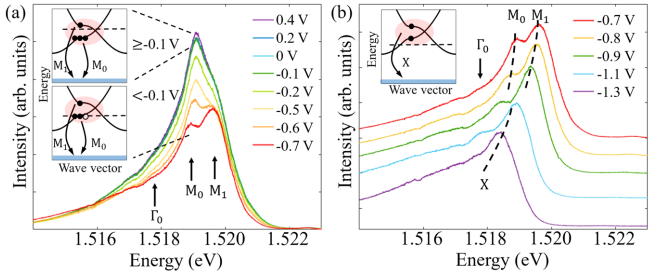

FIG. 4. (a) PL spectra in region AL. (b) PL spectra in the transition from AL to LDL regions. Insets: optical transitions at different voltage ranges. Filled and empty dots represent population changes in each flat band and the dashed red line marks E_F. The elliptical background denotes coupling between transitions. PL spectra of an unpatterned QW sharing the same contacts with the AG device show that its E_F is linear with V_b. In (b) at low n_e two excitonic transitions mix with each other and give a coupled excitonic transition (X). The large peak width comparable to the doublet energy splitting in (a) and (b) can be attributed to both thermal distribution of holes and electron-electron interactions. The lifetime broadening of electron states due to disorder is small (suggested by narrow intersubband RILS peaks), and the peak width does not represent the sharpness of AG DOS.

doublet is also the strongest optical emission at 10 K, which clearly reveals the presence of M_1 peak. The spectrum at 10 K is different from that at 5 K, which could be linked to Coulomb interaction effects, as we discuss below. Under higher temperatures, electrons at Γ point are thermally populated to higher levels, giving a lower intensity of the Γ_0 line. The doublet finally disappears above 20 K.

Remarkable changes in PL occur upon entering region AL where the Γ_0 line is replaced by the strong M_0-M_1 doublet emission. This evolution of PL spectra can be interpreted as arising from changes in the DOS when 2DES evolves from a quasiuniform status in region QU to an AG configuration in region AL where the DOS is given by honeycomb symmetry. The emergence of M_0-M_1 doublet in PL is continuous in the evolution from regions QU to AL (see Fig. S1 of Supplemental Material [20]). The energy of the M_0 line is 1 meV higher than that of the Γ_0 line, consistent with the situation that the singularity of the lower flat band is 1 meV higher than the CB around Γ point [see Fig. 1(e)]. The energy separation between M_0 and M_1 peaks is about 0.9 meV, close to that of vHSs [relevant optical transitions are shown in Fig. 2(b)]. Thus, we could attribute the M_0-M_1 doublet to the vHS doublet of AG flat bands. The explanation of the doublet splitting is supported by the density-functional study finding that key features of AG bands are stable against electron-electron interactions [21]. The carrier-density-dependent PL experiments reveal emerging vHSs and confirm the presence of AG flat bands. Previous resonant inelastic light scattering (RILS) experiments [9,12] that probe joint DOS between AG bands suggest that the two AG bands near M points are parallel, but cannot encode the energy dispersion of each single flat band (see Fig. S3 of Supplemental Material [20]).

The honeycomb symmetry of AG bands is linked to the constancy of doublet energies. As shown in Figs. 2(a) and 4(a), the PL doublet energies do not change in region AL, which could be interpreted in terms of the symmetry of the DOS singularity at M points of the BZ where there are six equivalent valleys sharing n_e. Figure 3 shows that n_e in region AL is typically about 4×10^{10} cm^{-2}. We estimate that n_e in each valley of the M_0 singularity is tuned down by V_b from 2.3×10^9 cm^{-2} when states of the M_0 singularity are fully populated, to nearly full depletion when E_F is below the singularity. This is a relatively small density variation that would not change the optical recombination energy of electrons in GaAs QWs [22,23].

The discussions above demonstrate that the energy properties of PL doublet can be captured by the single-particle picture based on honeycomb symmetry. Nevertheless, detailed PL spectra behaviors cannot be understood by single-particle physics. The line shapes of PL spectra in region AL cannot be described by calculations based on AG DOS. The intensity ratio of the M_0 line over the M_1 line in experiments is lower than those in single-particle calculations (see Fig. S4 of Supplemental Material [20]). Moreover, as shown in Fig. 4(a), the intensity of M_0 and M_1 transitions is fixed for $V_b > -0.1$ V, and their ratio is fixed across region AL. In a single-particle picture, this behavior indicates that the population ratio between M_0 and M_1 singularities is fixed, which is unlikely to happen because E_F sweeps from one singularity to another (see Fig. S5 of Supplemental Material [20]).

Many-body interactions, including exchange interactions in the flat band doublet, would play an important

role in understanding detailed PL spectra behaviors. In region AL, E_F stays between the singularity doublet (see Fig. 3), and the AG states are thus similar to those reported in Ref. [9], where large exchange interactions between AG bands (the exchange energy is about 0.6 meV $\approx$ 8 K) were reported. We could get some insight about this physics process from the Coulomb coupling between Fermi edge singularity and higher subband excitons [24–27]. Here the lower flat band is heavily populated while the upper flat band is weakly populated by thermal excitations and basically empty; thus the M_1-line intensity should be low under single-particle physics. However, the exchange energy between electrons in two flat bands is comparable with the splitting of flat bands, and Coulomb coupling would provide extra scattering channels from the lower flat band below E_F to the upper flat band. The strong coupling between the flat band doublet would contribute to a considerable luminescence intensity to M_1 singularity, and thus strengthens the ratio of the M_1-line intensity over the M_0-line intensity.

On the other hand, due to honeycomb symmetry, each valley has a small n_e. Under the small n_e born with the AG device, the Coulomb-interaction terms between the flat band doublet that are dominated by exchange coupling processes should have weak dependence on n_e and V_b [22,23]. Therefore, the doublet intensity is stable as long as the Coulomb coupling dominantly modifies the luminescence intensity. The striking stability of PL spectral line shapes in region AL suggests many-body interactions interplayed with symmetry of AG electrons. This can be confirmed by PL spectra under high temperatures. As shown in Fig. 2(d), for a higher temperature 10 K exceeding the exchange energy, the PL spectral line shape becomes unstable and the population ratio between M_0 and M_1 singularities changes. The larger M_1-line intensity at 10 K would be attributed to the major effect of excitons from thermally elevated electrons into the upper flat band [24]. A detailed line shape analysis should consider evolution of localized states and is out of the scope of this Letter.

The Coulomb coupling would be modulated as E_F crosses the lower flat band for $V_b < -0.1$ V (see Fig. 3). Figure 4(a) shows that the PL intensity starts to drop for $V_b < -0.1$ V, indicating the beginning of depopulation of M_0 singularity [see insets of Fig. 4(a)]. At $V_b < -0.9$ V, M_0 transition quickly collapses and the doublet evolves into one broad band labeled X [Fig. 4(b)]. The contrasting line shapes in regions LDL and AL indicate different underlying processes. At $V_b = -1.1$ V, E_F is well below M_0 singularity and the population of M_0-M_1 doublet is greatly reduced, so optical transitions from these states can be considered as excitonic. Instead of a doublet, band X in Fig. 4(b) indicates the mixture of excitonic transitions from each singularity by strong coupling between the doublet [9]. The attribution of band X to excitons is consistent with significant redshifts of its PL energies in region LDL [see Figs. 2(a) and 4(b)]. The operation of V_b to reduce n_e results in an increase of the electric field at the QW. Then the redshift could be understood in terms of a quantum-confined Stark effect of excitons [28] that brings redshifts of about 0.5 meV for electric field changes of 5×10^3 V/cm. We note that the appearance of excitonic transitions above E_F is not trivial and implies couplings between the Fermi sea and higher AG bands [24,25].

To summarize, flat bands are observed in carrier-density-dependent PL experiments in a backgated semiconductor AG device. PL spectra show striking dependence on carrier densities tuned by V_b, marked by three regions with contrasting spectral line shapes, and proves that the flat bands of semiconductor AG are accessible by E_F. Under appropriate flat bands population, Coulomb interactions within the flat band doublet are observed and take a critical role in stability of PL spectra. Several key features of semiconductor AG make it an excellent platform for further studies. For example, transport measurements could investigate many-body physics in the embedded flat bands, e.g., unconventional superconductivity [2,3,29]. Under strong magnetic fields [30], correlated phases such as Mott-Hubbard bands observed in honeycomb lattices [31] could promise novel collective behaviors. In general, compared with 2D moiré heterostructures, AG can be employed as a seminal quantum simulator of electron correlation operating in a rarely studied density regime.

The work at Columbia University was supported by the National Science Foundation, Division of Materials Research under Award No. DMR-1306976 and by Grant No. DE-SC0010695 funded by the U.S. Department of Energy Office of Science, Division of Materials Sciences and Engineering. Work at Nanjing University was supported by the Fundamental Research Funds for the Central Universities (Grant No. 14380146) and National Natural Science Foundation of China (Grant No. 12074177). This research is funded in part by the Gordon and Betty Moore Foundation's EPiQS Initiative, Grant No. GBMF9615 to L. N. P., and by the National Science Foundation MRSEC Grant No. DMR 1420541. Work at Purdue University was supported by the U.S. Department of Energy, Office of Science, Basic Energy Sciences, under Award No. DE-SC0006671.

L. D. and Z. L. contributed equally to this work.

*ljdu@nju.edu.cn
†ap359@columbia.edu

[1] J. González, Kohn-Luttinger superconductivity in graphene, Phys. Rev. B **78**, 205431 (2008).
[2] R. Nandkishore, L. S. Levitov, and A. V. Chubukov, Chiral superconductivity from repulsive interactions in doped graphene, Nat. Phys. **8**, 158 (2012).

[3] R. Nandkishore, R. Thomale, and A. Chubukov, Superconductivity from weak repulsion in hexagonal lattice systems, Phys. Rev. B **89**, 144501 (2014).
[4] R. Bistritzer and A. H. MacDonald, moiré bands in twisted double-layer graphene, Proc. Natl. Acad. Sci. U.S.A. **108**, 12233 (2011).
[5] Y. Cao, V. Fatemi, A. Demir, S. Fang, S. L. Tomarken, J. Luo, J. Sanchez-Yamagishi, K. Watanabe, T. Taniguchi, E. Kaxiras, R. Ashoori, and P. Jarillo-Herrero, Correlated insulator behaviour at half-filling in magic-angle graphene superlattices, Nature (London) **556**, 80 (2018).
[6] Y. Cao, V. Fatemi, S. Fang, K. Watanabe, T. Taniguchi, E. Kaxiras, and P. Jarillo-Herrero, Unconventional superconductivity in magic-angle graphene superlattices, Nature (London) **556**, 43 (2018).
[7] C. H. Park and S. G. Louie, Making massless Dirac Fermions from a patterned two-dimensional electron gas, Nano Lett. **9**, 1793 (2009).
[8] M. Gibertini, A. Singha, V. Pellegrini, M. Polini, G. Vignale, A. Pinczuk, L. N. Pfeiffer, and K. W. West, Engineering artificial graphene in a two-dimensional electron gas, Phys. Rev. B **79**, 241406(R) (2009).
[9] L. Du, S. Wang, D. Scarabelli, L. N. Pfeiffer, K. W. West, S. Fallahi, G. C. Gardner, M. J. Manfra, V. Pellegrini, S. Wind, and A. Pinczuk, Emerging many-body effects in semiconductor artificial graphene with low disorder, Nat. Commun. **9**, 3299 (2018).
[10] J. D. Watson, G. A. Csáthy, and M. J. Manfra, Impact of Heterostructure Design on Transport Properties in the Second Landau Level of In Situ Back-Gated Two-Dimensional Electron Gases, Phys. Rev. Applied **3**, 064004 (2015).
[11] S. Wang, D. Scarabelli, Y. Kuznetsova, S. Wind, A. Pinczuk, V. Pellegrini, M. J. Manfra, G. C. Gardner, L. N. Pfeiffer, and K. W. West, Observation of electron states of small period artificial graphene in nano-patterned GaAs quantum wells, Appl. Phys. Lett. **109**, 113101 (2016).
[12] S. Wang, D. Scarabelli, L. Du, Y. Kuznetsova, L. N. Pfeiffer, K. W. West, G. C. Gardner, M. J. Manfra, V. Pellegrini, S. Wind, and A. Pinczuk, Observation of Dirac bands in artificial graphene in small period nano-patterned GaAs quantum wells, Nat. Nanotechnol. **13**, 29 (2018).
[13] G. Li, A. Luican, J. M. B. Lopes dos Santos, A. H. Castro Neto, A. Reina, J. Kong, and E. Y. Andrei, Observation of Van Hove singularities in twisted graphene layers, Nat. Phys. **6**, 109 (2010).
[14] K. K. Gomes, W. Mar, W. Ko, F. Guinea, and H. C. Manoharan, Designer Dirac fermions and topological phases in molecular graphene, Nature (London) **483**, 306 (2012).
[15] A. Pinczuk, J. Shah, R. C. Miller, A. C. Gossard, and W. Wiegmann, Optical processes of 2D electron-plasma in GaAs-(AlGa)As heterostructures, Solid State Commun. **50**, 735 (1984).
[16] D. Kamburov, K. W. Baldwin, K. W. West, S. Lyon, L. N. Pfeiffer, and A. Pinczuk, Use of microluminescence as a contactless measure of the 2D electron density in a GaAs quantum well, Appl. Phys. Lett. **110**, 262104 (2017).
[17] Y. Chung, K. W. Baldwin, K. W. West, N. Haug, J. Wetering, M. Shayegan, and L. N. Pfeiffer, Spatial mapping of local density variations in two-dimensional electron systems using scanning photoluminescence, Nano Lett. **19**, 1908 (2019).
[18] L. N. Pfeiffer (private communication).
[19] L. Nádvorník, M. Orlita, N. A. Goncharuk, L. Smrčka, V. Novák, V. Jurka, K. Hruška, Z. Výborný, Z. R. Wasilewski, M. Potemski, and K. Výborný, From laterally modulated two-dimensional gas towards artificial graphene, New J. Phys. **14**, 053002 (2012).
[20] See Supplemental Material at http://link.aps.org/supplemental/10.1103/PhysRevLett.126.106402 for detailed PL spectra, comparison between PL and RILS, and single-particle calculations.
[21] E. Räsänen, C. A. Rozzi, S. Pittalis, and G. Vignale, Electron-Electron Interactions in Artificial Graphene, Phys. Rev. Lett. **108**, 246803 (2012).
[22] G. E. W. Bauer and T. Ando, Many-body effects on luminescence spectrum of modulation-doped quantum wells, Phys. Rev. B **31**, 8321 (1985).
[23] C. Delalande, G. Bastard, J. Orgonasi, J. A. Brum, H. W. Liu, M. Voos, G. Weimann, and W. Schlapp, Many-Body Effects in a Modulation-Doped Semiconductor Quantum Well, Phys. Rev. Lett. **59**, 2690 (1987).
[24] W. Chen, M. Fritze, A. V. Nurmikko, M. Hong, and L. L. Chang, Fermi-edge singularities and enhanced magneto-excitons in the optical spectra of GaAs/(Ga,Al)As single quantum wells, Phys. Rev. B **43**, 14738 (1991).
[25] W. Chen, M. Fritze, W. Walecki, A. V. Nurmikko, D. Ackley, J. M. Hong, and L. L. Chang, Excitonic enhancement of the Fermi-edge singularity in a dense two-dimensional electron gas, Phys. Rev. B **45**, 8464 (1992).
[26] P. Hawrylak, Coupling of excitons with excitations of the Fermi sea in asymmetric quantum wells, Phys. Rev. B **44**, 6262 (1991).
[27] The physics origin of the doublet reported in this Letter is different from Refs. [24–26] and a complete theoretical treatment should consider two Coulomb coupled flat bands with many-body enhancements at a small electron density.
[28] D. A. B. Miller, D. S. Chemla, T. C. Damen, A. C. Gossard, W. Wiegmann, T. H. Wood, and C. A. Burrus, Band-Edge Electroabsorption in Quantum Well Structures: The Quantum-Confined Stark Effect, Phys. Rev. Lett. **53**, 2173 (1984).
[29] T. Li, J. Ingham, and H. D. Scammell, Artificial graphene: Unconventional superconductivity in a honeycomb superlattice, Phys. Rev. Research **2**, 043155 (2020).
[30] A. Patanè, N. Mori, O. Makarovsky, L. Eaves, M. L. Zambrano, J. C. Arce, L. Dickinson, and D. K. Maude, Manipulating and Imaging the Shape of an Electronic Wave Function by Magnetotunneling Spectroscopy, Phys. Rev. Lett. **105**, 236804 (2010).
[31] A. Singha, M. Gibertini, B. Karmakar, S. Yuan, M. Polini, G. Vignale, M. Katsnelson, A. Pinczuk, L. N. Pfeiffer, K. W. West, and V. Pellegrini, Two-dimensional Mott–Hubbard electrons in an artificial honeycomb lattice, Science **332**, 1176 (2011).